

## Article

# Ion Composition of the Beam Plasma Generated by Electron-Beam Evaporation of Metals and Ceramic in the Forevacuum Range of Pressure

Andrey V. Tyunkov <sup>1</sup>, Efim M. Oks <sup>1,2</sup>, Yury G. Yushkov <sup>1</sup> and Denis B. Zolotukhin <sup>1,\*</sup>

<sup>1</sup> Department of Physics, Tomsk State University of Control Systems and Radioelectronics, 40 Lenin Ave, 634050 Tomsk, Russia; tyunkov84@mail.ru (A.V.T.); oks@fet.tusur.ru (E.M.O.); yushkov@mail.ru (Y.G.Y.)

<sup>2</sup> Institute of High Current Electronics SB RAS, 2/3, Akademichesky Ave, 634055 Tomsk, Russia

\* Correspondence: denis.b.zolotukhin@tusur.ru

**Abstract:** We present the results of measurements of the ion composition of the plasma generated by an accelerated electron beam in the forevacuum pressure range. It has been found that the main contribution to ionization processes comes from beam electrons. It has been shown that, during the electron-beam evaporation of metal or ceramic targets, the number of ions evaporated from the materials in the beam plasma significantly exceeds the number of ions produced from the residual atmosphere and admitted gases. Together, electron beams and beam-produced plasma can catalyze the processes of coatings deposition or modification of the surface layer of the samples.

**Keywords:** beam plasma; forevacuum pressure range; ion composition; evaporation of metals and ceramic



**Citation:** Tyunkov, A.V.; Oks, E.M.; Yushkov, Y.G.; Zolotukhin, D.B. Ion Composition of the Beam Plasma Generated by Electron-Beam Evaporation of Metals and Ceramic in the Forevacuum Range of Pressure. *Catalysts* **2022**, *12*, 574. <https://doi.org/10.3390/catal12050574>

Academic Editors: Li Lin and Carles Corbella

Received: 27 April 2022

Accepted: 21 May 2022

Published: 23 May 2022

**Publisher's Note:** MDPI stays neutral with regard to jurisdictional claims in published maps and institutional affiliations.



**Copyright:** © 2022 by the authors. Licensee MDPI, Basel, Switzerland. This article is an open access article distributed under the terms and conditions of the Creative Commons Attribution (CC BY) license (<https://creativecommons.org/licenses/by/4.0/>).

## 1. Introduction

During the transport of kilo-electron-volt electron beams in a forevacuum (1–100 Pa), a beam plasma is generated with an electron density  $n_e \approx 10^9\text{--}10^{12}\text{ cm}^{-3}$  and a temperature  $T_e \approx 1.5\text{ eV}$  [1,2]. Such plasma is a convenient tool for catalyzing the process of nitrating metals, due to the efficient breakdown of nitrogen molecules into atoms by the electron beam [3–5]. The high efficiency of molecular dissociation and ionization in the beam plasma, as well as the steady positive potential of the plasma [6], make such plasma attractive for applications in the ion plasma modification of materials. Additionally, in the forevacuum pressure range, the beam plasma ions' neutralization of electric charges on the surfaces of nonconductive materials makes possible a direct electron-beam modification of dielectric materials. It is of practical interest to use electron-beam evaporation of high-temperature ceramics with ensuing ionization of the evaporated material and synthesis of dielectric coatings [7–9].

The beam plasma ion composition during the electron-beam evaporation of a solid target has an effect on the formation of coatings and their parameters. It is, therefore, important to have reliable measurements of the beam plasma ion composition and identify the main physical mechanisms responsible for ionization processes in the plasma.

The purpose of this work was to carry out experimental studies and numerical estimates related to measurements of the beam plasma ion composition, and to determine the contribution of beam and plasma electrons to the ionization processes of plasma generation in the forevacuum range of operating pressures, as well as to study the effect of the metal and ceramic vapor produced by the electron beam on the ion composition of plasma.

## 2. Experimental Results

Figure 1 shows the experimental results for the mass spectra studies of gas vapor ions conducted on the installation equipped with a high-vacuum pumping system (Figure 1a–c)

and with a forevacuum pumping system (Figure 1d). As seen below, in both cases, the ratio of the number of ions (the area of the peak) of the operating gases in the pair practically coincides with the ratio of ionization probabilities by the beam electrons of the corresponding gases (see Table 1). The calculation of the ratio of probabilities included all ions of the pairs of gases, as shown in Figure 1.

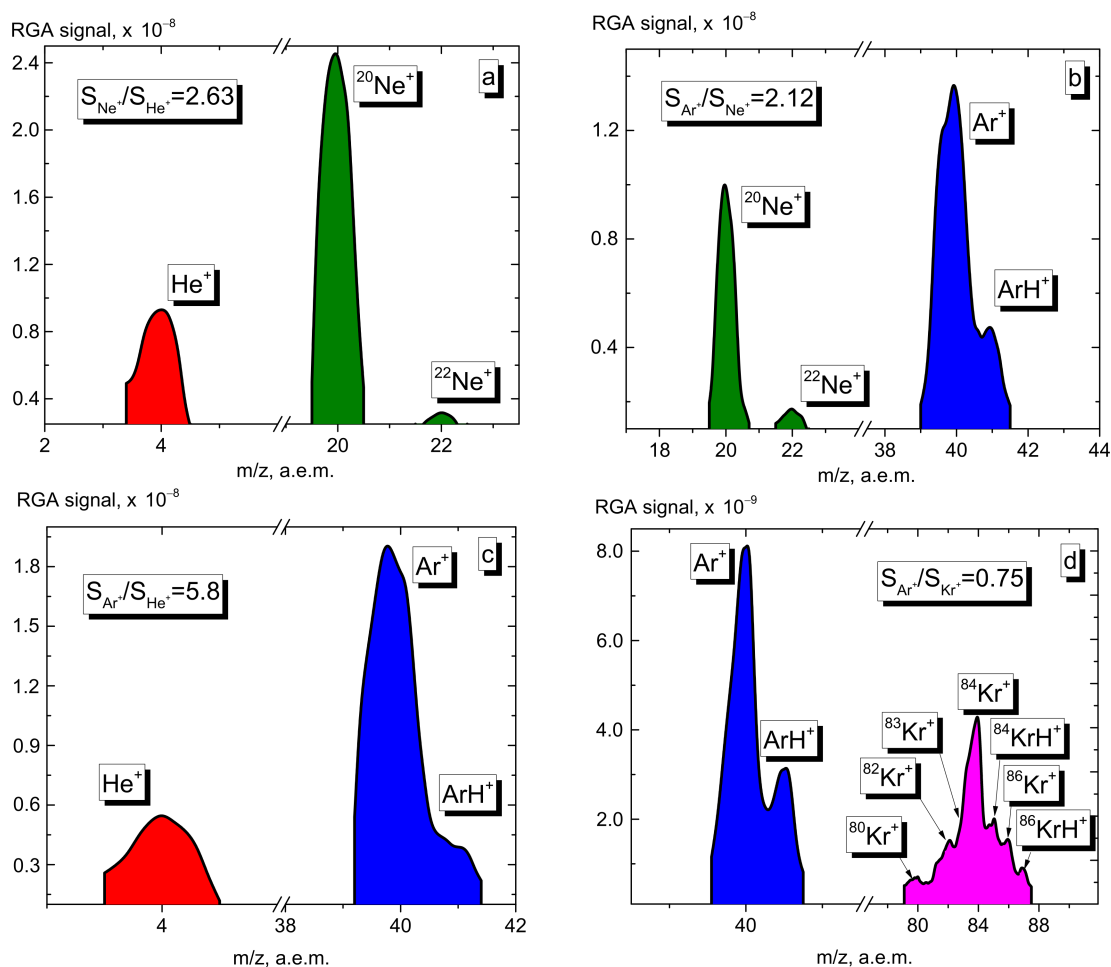


**Figure 1.** Mass spectra of gas pair ions obtained with high-vacuum (a–c) and fore-vacuum (d) pumping systems.

**Table 1.** Estimated ion composition in different inert gas mixtures.

Pair	$C_{i1}/C_{i2}$	$\sigma_{i1}/\sigma_{i2}$	$P_1/P_2$ (Plasma)	$P_1/P_2$ (Beam)	$N_1/N_2$ (Figure 1, Experiment)
Ar-He	2.0/0.13	1/0.19	3677	5.26	5.80
Ar-Ne	2.0/0.16	1/0.46	454	2.17	2.12
Ar-Kr	2.0/5.0	1/1.15	0.13	0.86	0.75
Ne-He	0.16/0.13	0.46/0.19	8.1	2.42	2.63

This fact indicates that ionization of beam plasma occurs predominantly due to high-energy beam electrons. It should be noted that the ratio of the numbers of ions corresponds to the ratio of the probabilities of their ionization under conditions of both high-vacuum pumping and fore-vacuum pumping. Thus, the quality of vacuum does not ultimately affect the ionization mechanism. Figure 2 shows the effects of the vapor of different metals and alumina ceramics on the transformation of the mass spectra of gas plasma. For all evaporated materials used in these experiments, the spectra show the dominance of ions

of evaporated material over gas ions. Since the power density of the electron beam was fixed for all beam positions, we attribute the difference in the signal amplitudes during the metal evaporation (Ti, Fe, Cu) to the difference in their melting temperatures ( $T_{\text{Ti}} = 1668\text{ }^{\circ}\text{C}$ ,  $T_{\text{Fe}} = 1538\text{ }^{\circ}\text{C}$ ,  $T_{\text{Cu}} = 1085\text{ }^{\circ}\text{C}$ ).

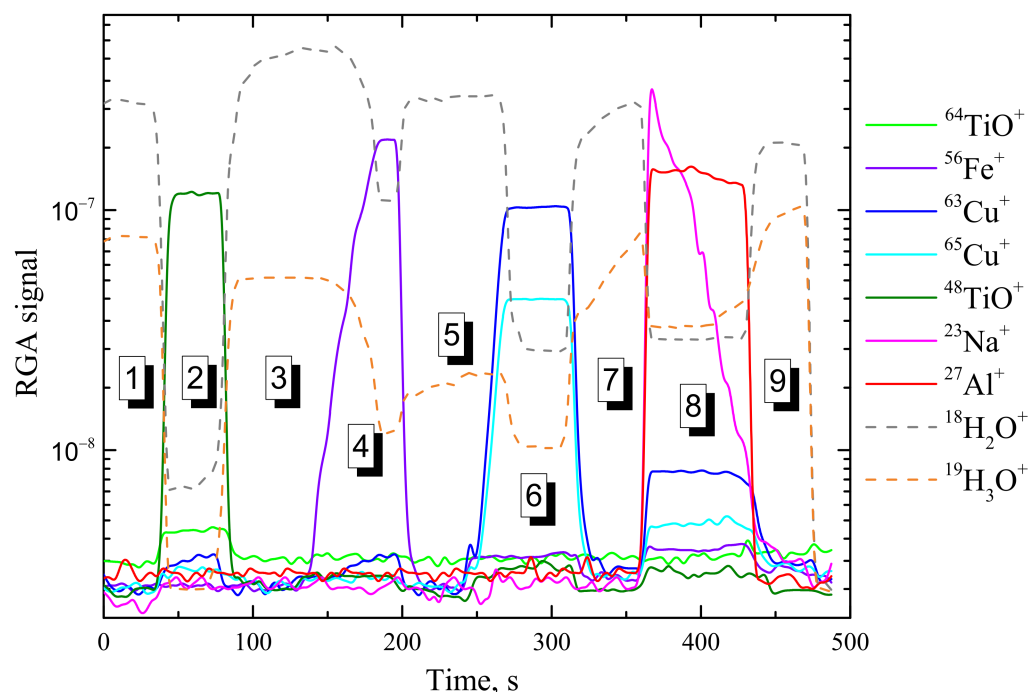


**Figure 2.** Mass spectra of the beam plasma ions during successive evaporation of solid targets. Numbers denote the electron beam positions as indicated in Section 3.

In the case of evaporated alumina ceramics, the predominant ions are of aluminum and sodium, despite the sodium content in the ceramics being as low as a few percent. It should be noted that the graphs in Figure 2 are plotted in absolute units, so the increase in the number of ions of the residual atmosphere cannot be related with an increase in the density of evaporated materials.

To explain this fact, we make use of the results obtained in the first part of our work. According to these results, the number of ions in the beam plasma essentially depends on the ionization cross-section of atoms and molecules under consideration. Let us consider the ionization cross-sections of our evaporated materials (Figure 3) obtained by different authors [10–12]. As seen in Figure 3, the ionization cross-section of water molecules is significantly lower than that of any of the presented elements; accordingly, the ionization probability of water vapor molecules is less than the ionization probabilities of metal vapors. This explains the sharp decrease in water vapor ions in the spectrum when metal vapors are present in the plasma, and the recovery of the original picture when they are absent.

In the case of evaporated alumina ceramics, the spectrum predominantly recorded ions of atomic sodium and aluminum, along with a small number of clusters based on them ( $\text{AlO}^+$  and  $\text{Al}_2\text{O}^+$ ,  $\text{NaO}^+$ ), which is in qualitative agreement with our previous experiments [13]. The initial rise in the number of sodium ions in Figure 2 is due to its low melting temperature ( $97.79\text{ }^{\circ}\text{C}$ ), while the drop is due to the rapid evaporation of small amount of sodium from the bulk of the material. Note that the small amplitude of  $\text{AlO}^+$  cluster ions does not signify the presence of a small amount of corresponding neutrals in the total flux, since the ionization cross-section of  $\text{AlO}$  molecules is smaller than that of  $\text{Al}$  atoms by a factor of almost 2.5, while the ionization potential is higher by almost 4 eV [14]. The aforementioned facts indicate that the ionic composition of beam-produced plasma can be freely controlled by changing both the parameters of the measured beam

(energy and current) and the material of the target to be evaporated. This can be used as a catalyst for increasing the coatings deposition rate, as well as for the modification of the coatings' structure and properties, due to the directed action of the ion flux onto the processing substrate.

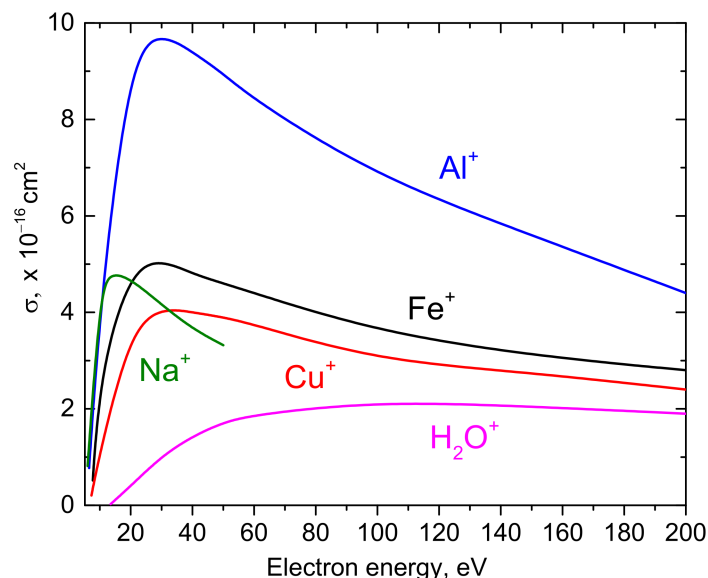


**Figure 3.** Electron-impact ionization cross-section of metal atoms and water molecules [10–12].

### 3. Experimental Setup and Technique

The first set of experiments was aimed at revealing the role of plasma and beam electrons in the ionization of the operating gas and, accordingly, in the generation of the beam plasma. The idea behind the experiment was to admit a pair of inert gases (argon-helium, argon-neon, neon-helium, and argon-krypton) into the vacuum chamber with an equal partial pressure of about 1 Pa. Inert gases were chosen in order to exclude the effect of dissociation. The selected gases in each pair had sharp differences in the ionization potentials and cross-sections (argon-helium, argon-neon). To eliminate the effect of Penning ionization, we used the gas pairs (helium-neon, argon-krypton) with ionization potentials above the excitation energy of metastable levels.

During the beam plasma generation, we measured the ion composition of plasma and determined the ratio of the ion components of the particular gas pair. This ratio was compared with theoretical estimates of the ratio of ionization probabilities of the given pair of gases by plasma and beam electrons. The temperature of plasma electrons was assumed to be 1.5 eV [1] and the electron energy distribution to be Maxwellian.

The experimental setup is shown in Figure 4. The beam plasma was generated using a forevacuum hollow-cathode plasma electron source, operating in a continuous mode. A detailed description and the working principle are discussed in [15]. At an accelerating voltage of 10 kV, the electron beam current was maintained at a level of 50 mA. The plasma ion composition was measured with an RGA-300 residual atmosphere quadrupole mass spectrometer (Residual Gas Analyzer, Stanford Research Systems, Sunnyvale, CA, USA). When conducting the experiments, we replaced the analyzer ionizer with a two-electrode ion-optical system to extract ions from the beam plasma (Figure 5). As opposed to the previous design of the mass spectrometer [16], the electrodes were made of stainless steel with a higher temperature resistance. The extraction plate and the drift tube were combined into one extracting electrode. This solution enabled us to reduce the number of insulators and sealings between the electrodes in the ion extraction region where the temperature was maximal.

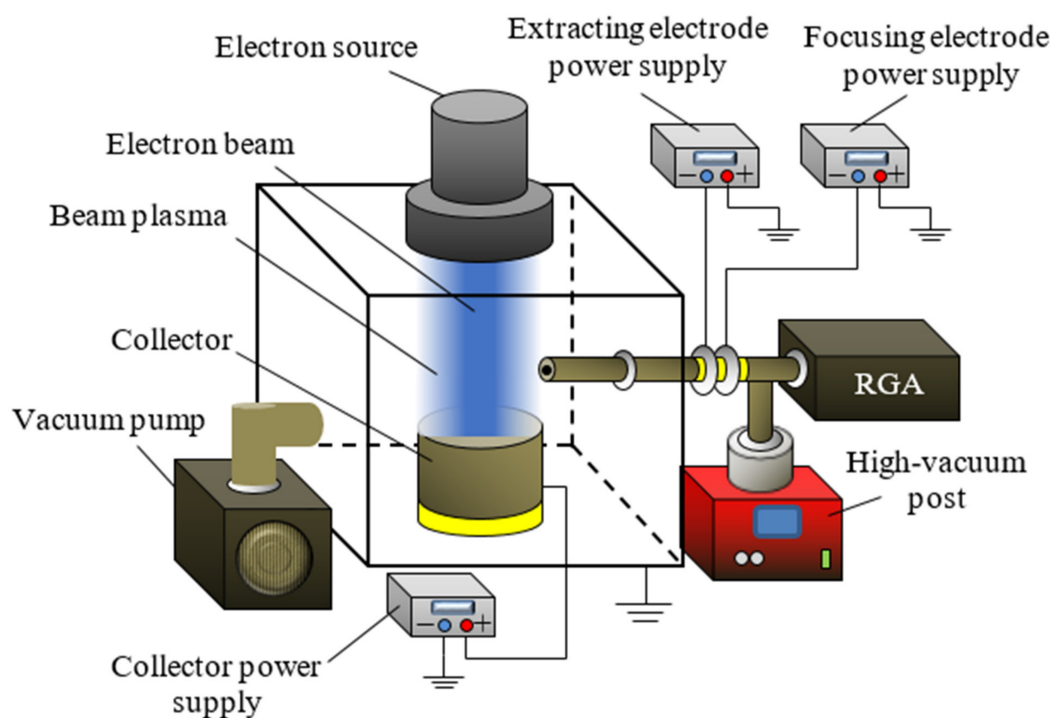


Figure 4. Schematic diagram of the experimental setup.

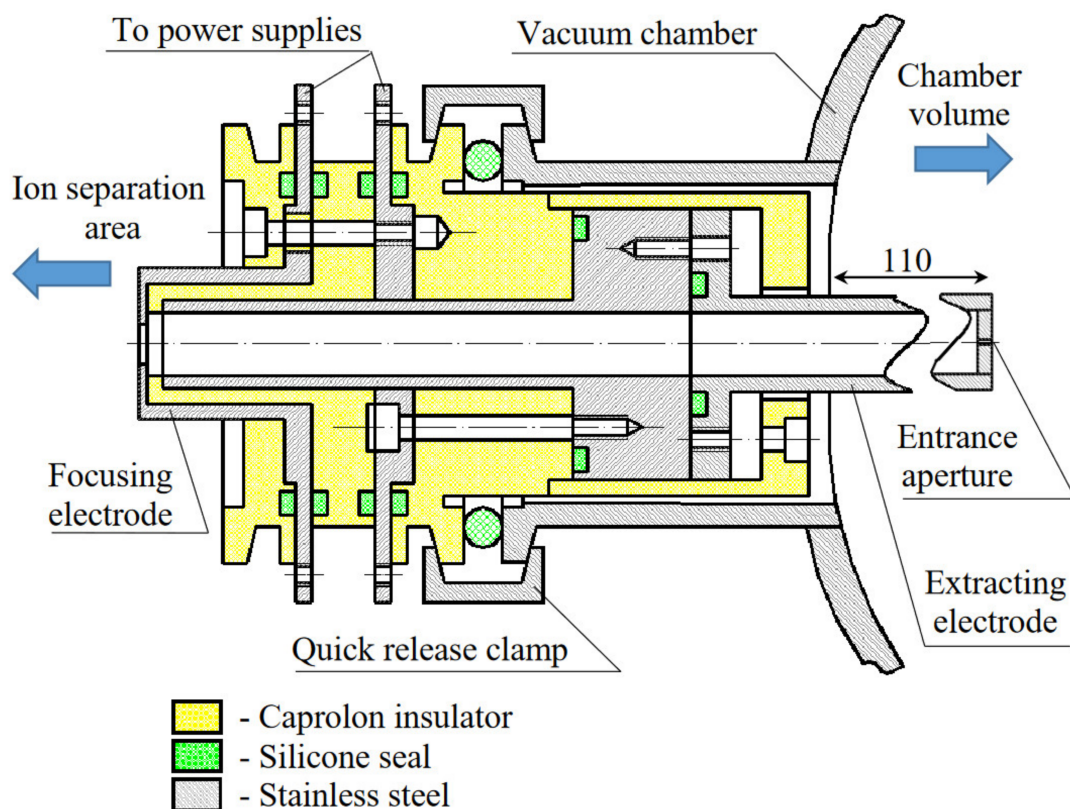


Figure 5. Schematic diagram of the mass spectrometer ion-optical system.

The extracting electrode is a thin-walled tube with one end shut by a 2 mm thick plate with a small hole of  $\varnothing 0.6$  mm. This electrode provides the ion flux transport from its generation region (the area of the electron beam's interaction with the target) to the separation region (quadrupole rods of the mass analyzer). In this case, despite the chamber

pressure of a few pascals, due to the pressure drop at the entrance aperture of small diameter, the extracted ions are transported at a pressure no greater than  $10^{-2}$  Pa. The ion flux separation region was additionally evacuated by a vacuum post HiCube 80 Eco (Pfeiffer Vacuum, Wetzlar, Germany) at a pumping rate of 67 L/s. In order to exclude foreign impurities, the spectrometer ion-optical system was designed in such a way that the current leads to electrodes were located outside the vacuum chamber. As a result, this system was able to withstand continuous operation at a high heat load when generating the beam plasma and evaporating the solid target with the electron beam.

Since the current-receiving part of the mass analyzer is at the ground potential, and the beam plasma potential is positive of a few volts [6], for the beam plasma ions to reach the current-receiving part, a positive potential of 17 V relative to the ground was applied to the electron beam collector (a heavy iron cylinder, 85 mm high and 65 mm in diameter). To direct the ion flux to the separation region (quadrupole rods of the mass analyzer), a negative bias potential of 12 V was applied to the extracting and focusing electrodes of the extracting ion-optical system.

In order to determine the effect of the residual atmosphere on the ionization mechanism, parts of the experiments were carried out on the installation equipped with an oil-free pumping system: a nEXT300D turbomolecular pump with a pumping rate of 300 L/s (Edwards Ltd., Burgess Hill, West Sussex, UK). As a result, the chamber was evacuated to the limiting pressure 0.027 Pa. This installation was used to study the spectra of the following mixtures: neon-helium, neon-argon, and argon-helium. The argon-krypton spectrum was studied using the installation with one pumping stage. The vacuum was provided by a BOC Edwards E2M80 (Edwards Ltd., Burgess Hill, West Sussex, UK) mechanical rotary vane pump with a pumping rate of 20 L/s. The limiting residual pressure in this case was 1.7 Pa.

Since we actively use the forevacuum plasma electron source to deposit coatings based on electron-beam evaporation of various metals [17] and alumina ceramic [7], the second set of experiments was devoted to studying the effect of the material vapor on the ion composition of the beam plasma.

To this end, graphite crucibles were mounted on the electron beam collector of the experimental installation with one pumping stage. Fragments of various metals (titanium, iron, copper) and alumina ceramics were put inside the crucibles. Numbers in Figure 6 show the positions of the electron beam at different moments of time.

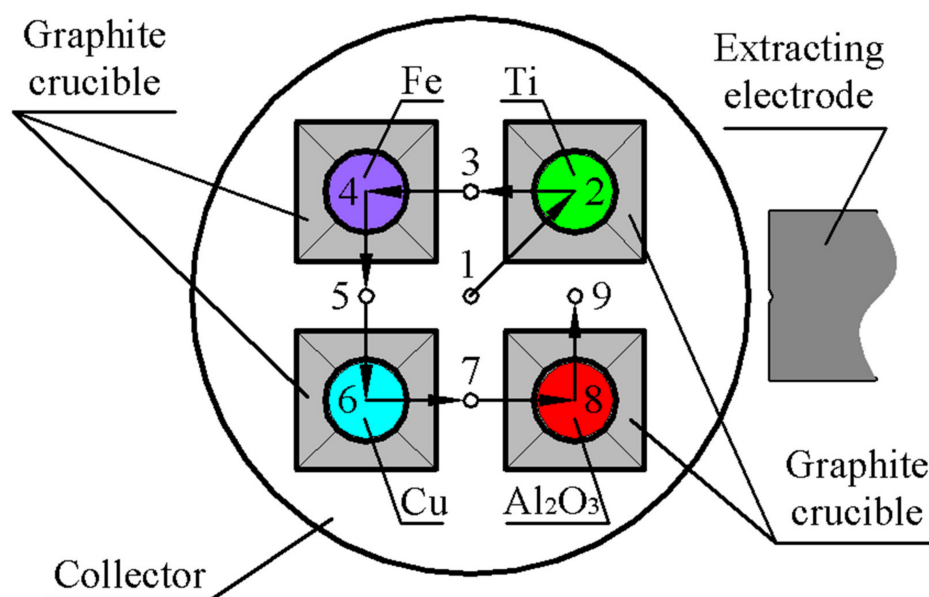


**Figure 6.** Experimental setup for studying mass spectra during the evaporation of solid targets (view from above).

In these experiments, the energy of accelerated electrons was maintained at a level of 7 keV; the beam current was 100 mA; the operating gas pressure (in this case helium) was 5 Pa.

#### 4. Estimation of the Contribution of Plasma Electrons and Beam Electrons to Ionization

The contributions of two groups of electrons determine the steady state ion composition of the plasma, which can be measured using a mass-to-charge spectroscopy technique. Moreover, by comparing the measured ion composition of the plasma with the estimates of the ionization probabilities of each of the gas mixture components, one can make a conclusion as to which electron group is the major contributor to the beam plasma generation.

To estimate the role of plasma electrons in the beam plasma formation for a given gas pair, let us use the known expression for the ionization output  $\nu_i$  at electron energies close to the ionization energy. This expression is derived assuming a Maxwellian distribution of electron energy, and a linear approximation of the dependence of the electron impact ionization cross-section on the electron energy [18]

$$\nu_i = n_e \cdot n_a \cdot C_i \cdot \left( \frac{8kT_e}{\pi m_e} \right) \cdot (U_i + 2kT_e) \cdot \exp\left(-\frac{U_i}{kT_e}\right), \quad (1)$$

where  $C_i$  is a constant in the linear dependence of the ionization cross-section on temperature,  $n_a$  is the number density of gas molecules,  $n_e$  is the number density of electrons, and  $U_i$  is the ionization potential.

At equal partial pressures of the gas mixture components, the ratio of ionization probabilities  $P_1$  and  $P_2$  is reduced to the ratio of their ionization rates

$$\frac{P_1}{P_2} = \frac{\nu_{i1}}{\nu_{i2}} = \frac{C_{i1}}{C_{i2}} \cdot \left( \frac{U_{i1} + 2kT_e}{U_{i2} + 2kT_e} \right) \cdot \exp\left(\frac{U_{i2} - U_{i1}}{kT_e}\right). \quad (2)$$

The beam electrons have practically the same energy, which significantly exceeds the energy corresponding to the maximum ionization cross-section. In this case, the ratio of the electron-beam ionization probabilities is determined by the ratio of ionization cross-sections of the gas pair at a fixed electron energy.

We use the Lotz approximation for ionization of an atom from the ground state [19,20].

$$\sigma(E) = \sum_{i=1}^N a_i q_i \frac{\ln \frac{E}{U_a}}{E \cdot U_a} \times \left\{ 1 - b_i \exp\left(-c_i \left(\frac{E}{U_a} - 1\right)\right) \right\}, \quad (3)$$

where  $a$ ,  $b$ ,  $c$  are constants of the empirical formula [20],  $q_i$  is the number of equivalent shell electrons,  $E$  is the electron energy, and  $U_a$  is the ionization potential.

The results of the estimates and measured values of the ion composition of all of the gas pairs used in the experiments are summarized in Table 1. The estimates are made for a plasma electron temperature of 1.5 eV and an electron beam energy of 10 keV.

The results of this study will be useful for scientists working on applied research in the field of deposition of various types of ceramic-metal coatings using the electron-beam method. The findings regarding the ionic composition of the beam plasma will make it possible to effectively control the rates of coating deposition as well as their composition.

#### 5. Conclusions

As a result of our studies of the ion composition of the plasma generated by an accelerated electron beam in the forevacuum pressure range, we have found that the major contribution to ionization comes from high-energy beam electrons. During electron-beam evaporation of metal or ceramic targets, the number of ions of the evaporated material in the beam plasma is much greater than the number of ions of the residual atmosphere and admitted gasses due to the larger ionization cross section. Thus, in the forevacuum range

of pressure, despite the presence of a large quantity of gas molecules, and even water, in the residual atmosphere, electron-beam evaporation of metals and ceramic can effectively generate the beam plasma that contains mostly ions of evaporated material. The obtained results demonstrate the benefits of using electron-beam evaporation of conductive and dielectric materials in a forevacuum for creating various functional and protective coatings.

**Author Contributions:** Conceptualization, A.V.T. and Y.G.Y.; methodology, D.B.Z.; validation, A.V.T., Y.G.Y. and D.B.Z.; investigation, A.V.T.; data curation, A.V.T.; writing—original draft preparation, A.V.T.; writing—review and editing, Y.G.Y.; visualization, D.B.Z.; supervision, E.M.O.; project administration, E.M.O.; funding acquisition, E.M.O. All authors have read and agreed to the published version of the manuscript.

**Funding:** This research was funded by Russian Science Foundation grant number 21-79-10035.

**Data Availability Statement:** Data supporting research is available upon reasonable request.

**Conflicts of Interest:** The authors declare no conflict of interest.

## References

1. Zolotukhin, D.B.; Burdovitsin, V.A.; Oks, E.M.; Tyunkov, A.V.; Yushkov, Y.G. On the influence of electron-beam metal evaporation on parameters of beam plasma in medium vacuum. *Phys. Plasmas* **2019**, *26*, 053512. [[CrossRef](#)]
2. Leonhardt, D.; Walton, S.G.; Blackwell, D.D.; Amatucci, W.E.; Murphy, D.P.; Fernsler, R.F.; Meger, R.A. Plasma diagnostics in large area plasma processing system. *J. Vac. Sci. Technol. A* **2001**, *19*, 1367–1373. [[CrossRef](#)]
3. Fernsler, R.F.; Manheimer, W.M.; Meger, R.A.; Mathew, J.; Murphy, D.P.; Pechacek, R.E.; Gregor, J.A. Production of large-area plasmas by electron beams. *Phys. Plasmas* **1998**, *5*, 2137–2143. [[CrossRef](#)]
4. Muratore, C.; Walton, S.G.; Leonhardt, D.; Fernsler, R.F.; Blackwell, D.D.; Meger, R.A. Effect of plasma flux composition on the nitriding rate of stainless steel. *J. Vac. Sci. Technol. A* **2001**, *22*, 1530–1535. [[CrossRef](#)]
5. Muratore, C.; Leonhardt, D.; Walton, S.G.; Blackwell, D.D.; Fernsler, R.F.; Meger, R.A. Low-temperature nitriding of stainless steel in an electron beam generated plasma. *Surf. Coat. Technol.* **2005**, *191*, 255–262. [[CrossRef](#)]
6. Walton, S.G.; Leonhardt, D.; Blackwell, D.D.; Fernsler, R.F.; Murphy, D.P.; Meger, R.A. Ion energy distributions in a pulsed, electron beam-generated plasma. *J. Vac. Sci. Technol. A* **2001**, *19*, 1325–1329. [[CrossRef](#)]
7. Yushkov, Y.G.; Oks, E.M.; Tyunkov, A.V.; Zolotukhin, D.B. Alumina coating deposition by electron-beam evaporation of ceramic using a forevacuum plasma-cathode electron source. *Ceram. Int.* **2019**, *45*, 9782–9787. [[CrossRef](#)]
8. Yushkov, Y.G.; Tyunkov, A.V.; Oks, E.M.; Zolotukhin, D.B. Electron beam evaporation of boron at forevacuum pressures for plasma-assisted deposition of boron-containing coatings. *J. Appl. Phys.* **2016**, *120*, 233302. [[CrossRef](#)]
9. Yushkov, Y.G.; Oks, E.M.; Tyunkov, A.V.; Zolotukhin, D.B. Dielectric Coating Deposition Regimes during Electron-Beam Evaporation of Ceramics in the Fore-Vacuum Pressure Range. *Coatings* **2022**, *12*, 1305. [[CrossRef](#)]
10. Johnston, A.R.; Burrow, P.D. Electron-impact ionization of Na. *Phys. Rev. A* **1995**, *51*, R1735–R1737. [[CrossRef](#)] [[PubMed](#)]
11. Freund, R.S.; Wetzel, R.C.; Shul, R.J.; Hayes, T.R. Cross-section measurements for electron-impact ionization of atoms. *Phys. Rev. A* **1990**, *41*, 3575–3595. [[CrossRef](#)] [[PubMed](#)]
12. Itikawa, Y.; Mason, N. Cross sections for electron collisions with water molecules. *J. Phys. Chem. Ref. Data* **2005**, *34*, 1–22. [[CrossRef](#)]
13. Yushkov, Y.G.; Zolotukhin, D.B.; Oks, E.M.; Tyunkov, A.V. Different stages of electron-beam evaporation of ceramic target in medium vacuum. *J. Appl. Phys.* **2020**, *127*, 113303. [[CrossRef](#)]
14. Deutsch, H.; Hilpert, K.; Becker, K.; Probst, M.; Märk, T.D. Calculated absolute electron-impact ionization cross sections for AlO, Al<sub>2</sub>O, and WO<sub>x</sub> (x = 1–3). *J. Appl. Phys.* **2001**, *89*, 1915–1921. [[CrossRef](#)]
15. Burdovitsin, V.A.; Oks, E.M. Fore-vacuum plasma-cathode electron sources. *Laser Part. Beams* **2008**, *26*, 619–635. [[CrossRef](#)]
16. Zolotukhin, D.B.; Tyunkov, A.V.; Yushkov, Y.G.; Oks, E.M. Modified quadrupole mass analyzer RGA-100 for beam plasma research in forevacuum pressure range. *Rev. Sci. Instrum.* **2015**, *86*, 123301. [[CrossRef](#)] [[PubMed](#)]
17. Zolotukhin, D.B.; Oks, E.M.; Tyunkov, A.V.; Yushkov, Y.G. Deposition of dielectric films on silicon using a fore-vacuum plasma electron source. *Rev. Sci. Instrum.* **2016**, *87*, 063302. [[CrossRef](#)] [[PubMed](#)]
18. Levitsky, S.M. *Collection of Problems and Calculations in Physical Electronics*; Kiev University Press: Kiev, Ukraine, 1964; 209p.
19. Lotz, W. Electron-impact ionization cross-section for atoms up to Z = 108. *Z. Phys.* **1970**, *232*, 101–107. [[CrossRef](#)]
20. Lotz, W. An Empirical Formula for the Electron-Impact Ionization Cross-Section. *Z. Phys.* **1967**, *206*, 205–211. [[CrossRef](#)]